

On the Optimum Die Shape in Rod Drawing Process Considering Work-Hardening Effect of Material

M.M. Mahdavi, H. Haghghat *

Mechanical Engineering Department, Razi University, Kermanshah, Iran

Received 28 May 2020; accepted 3 July 2020

ABSTRACT

The assessment of the influence of the work-hardening of material on the optimum die profile and drawing force in rod drawing process is the main objective of the present paper. The upper bound solution, based on the assumption of perfect plasticity, has been extended to consider the work hardening of the material during the rod drawing process through curved dies. Analytical results of drawing forces for rod drawing process through four different types of streamlined die profiles are compared with the finite element simulation data using the finite element code DEFORM 2D. It is shown that as the work-hardening exponent increases, the optimum die length increases, the required drawing force decreases and maximum possible reduction in area increases. Based on this proposed modeling technique, drawing process of real materials through various curved dies can be optimized.

© 2020 IAU, Arak Branch. All rights reserved.

Keywords: Rod drawing; Work hardening; Upper bound analysis.

1 INTRODUCTION

DURING rod drawing, raw material is pulled through a die in order to reduce its diameter. Pulling of rod material is done by applying of the tensile force to the rod at the exit side of the die. Optimization of die profile has been one of the most important tasks that have attracted the attention of many researchers. Richmond and Devenpeck [22] proposed ideal die geometry for strip drawing under the assumption of no work-hardening material and frictionless die. Avitzur [1-2] applied the upper bound theorem to the wire drawing through conical dies assuming perfect plasticity for the material. Using slip line analysis, Devenpeck and Richmond [6] designed streamlined sigmoidal dies that would theoretically produce an extruded strip with no distortion. Chen and Ling [3] and Nagpal [16] developed velocity fields for axisymmetric extrusions through arbitrarily shaped dies. Chen et al. [4] and Liu and Chung [13] used finite element analysis to examine wire drawing through conical dies. Yang et al. [23] and Yang and Han [24] developed upper bound models with streamlined sigmoidal shaped dies. Chevalier [5] investigated the effect of geometric parameters and the friction condition on the quality of the final wire using finite element simulation. Zhao et al. [25] proposed two kinematically admissible velocity fields through elliptic dies. Lu

*Corresponding author. Tel.: +98 83 34274530; Fax: +98 83 34274542.
E-mail address: hhaghghat@razi.ac.ir (H. Haghghat).

and Lo [14] used slab method to account for friction and material property changes in the deformation zone. A comparative study between analytical models and FEM results presented by Luis et al. [15] in order to obtain the required drawing force s , stresses and strains which are involved in the wire drawing process. Ponalagusamy et al. [17] designed streamlined dies based on Bezier curves and polynomial equations and compared them with each other for perfectly plastic materials. Chen and Huang [7] used the finite element and the Taguchi methods to optimize the process parameters of the wire drawing process. Gordon et al. [8-9-10] developed an adaptable die design method for axisymmetric extrusion of perfectly plastic materials. They found that their proposed die profile is superior to the streamlined die shape of Yang and Han [24]. An attempt made by Panteghini and Genna [18] to consider the strain-hardening effects on optimization of wire drawing process through conical dies. Rubio et al. [20] developed an analytical solution for sheet drawing process assuming a perfect plastic material under plane strain condition. Gonzalez et al. [11] used the slab method and the finite element method to prediction the drawing force necessary to carry out a rod drawing process of a rigid-plastic material. Rubio et al. [21] extended their solution of plate drawing, which presented in Rubio et al. [20], to consider the material work hardening but it was relatively simple. An upper bound solution to estimate the drawing stress in plate drawing processes has been developed by Panteghini [19]. Zhang et al. [26] studied the rod drawing through a twin parabolic die by upper bound method, assuming perfect plasticity for the rod material.

Most of research work reviewed above performed on the optimization of die geometry by the upper bound method under the assumption of a perfect plastic material. However, to design optimal die shapes in general depends on the predictions of actual metal flow characteristics within the die under the given process conditions and real materials. The main objective of the present paper is the assessment of the influence of the work-hardening behavior of material on the optimum die of prescribed profile. A velocity field and upper bound solution, based on the assumption of perfect plasticity, have been extended to consider the work hardening of the material. The effective strain and the flow stress have been calculated for each particle on the shear surfaces and in the deformation region. Several different shapes of the die have been performed and performance comparison is made among them.

2 UPPER BOUND ANALYSIS

Fig. 1 shows a schematic diagram of the rod drawing through a die of curved profile shape. As shown in this figure, the material starts as a round section rod of radius R_o and is drawn into a cylindrical rod of radius R_f . Angle α is the angle of the line connecting the initial point of the curved die to the final point of the die and $\tan \alpha = (R_o - R_f) / L$, where L is die length. The die surface, which is labeled as $\psi(r)$ in Fig. 1, is given in the spherical coordinate system. For the conical die shape, this function has a single constant value, i.e. $\psi(r) = \alpha$.

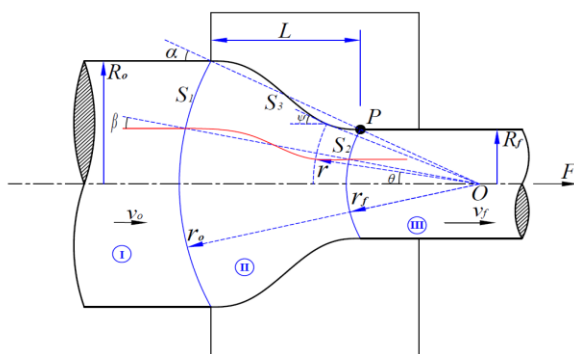


Fig.1
Schematic diagram of rod drawing process through a curved die using spherical coordinate system and deformation regions.

To analyze the process, the material under deformation is divided into three regions, as shown in Fig. 1. A spherical coordinate system (r, θ, ϕ) is used to describe the position of the two shear surfaces S_1 and S_2 as well as the velocity in region II. The surface S_1 is located at distance r_o from the origin and the surface S_2 is located at distance r_f from the origin. The position of the coordinate system origin, point O , is defined by the intersection of a line that goes through the start and end points of the die profile, with the die axis. In region I, the incoming material

is assumed to flow horizontally as rigid body with velocity v_o . In region III, the material is assumed to flow horizontally as rigid body with velocity v_f . Region II is the deformation region, where the velocity is complex.

2.1 Velocity field in deformation region

The velocity field in region II in spherical coordinates is similar to the one assumed by Gordon et al. [8] for rod extrusion through a curved die as:

$$V_r = -v_f \left(\frac{r_f}{r} \right)^2 \frac{\sin^2 \alpha}{\sin^2 \psi} \cos \theta \quad (1)$$

$$V_\theta = -v_f \frac{r_f^2}{r} \frac{\partial \psi}{\partial r} \left(\frac{\sin \alpha}{\sin \psi} \right)^2 \frac{\sin \theta}{\tan \psi} \quad (2)$$

where v_f is velocity of drawn rod.

The strain rates in spherical coordinates are defined as:

$$\begin{aligned} \dot{\epsilon}_{rr} &= \frac{\partial V_r}{\partial r} \\ \dot{\epsilon}_{\theta\theta} &= \frac{1}{r} \frac{\partial V_\theta}{\partial \theta} + \frac{V_r}{r} \\ \dot{\epsilon}_{\varphi\varphi} &= \frac{1}{r \sin \theta} \frac{\partial V_\varphi}{\partial \varphi} + \frac{V_r}{r} + \frac{V_\theta}{r} \cot \theta \\ \dot{\epsilon}_{r\theta} &= \frac{1}{2} \left(\frac{\partial V_\theta}{\partial r} - \frac{V_\theta}{r} + \frac{1}{r} \frac{\partial V_r}{\partial \theta} \right) \\ \dot{\epsilon}_{\theta\varphi} &= \frac{1}{2} \left(\frac{1}{r \sin \theta} \frac{\partial V_\theta}{\partial \varphi} + \frac{1}{r} \frac{\partial V_\varphi}{\partial \theta} - \frac{\cot \theta}{r} V_\varphi \right) \\ \dot{\epsilon}_{\varphi r} &= \frac{1}{2} \left(\frac{\partial V_\varphi}{\partial r} - \frac{V_\varphi}{r} + \frac{1}{r \sin \theta} \frac{\partial V_r}{\partial \varphi} \right) \end{aligned} \quad (3)$$

where $\dot{\epsilon}_{ij}$ (with $i \neq j$) is a shear strain rate component.

Based on the velocity field, the strain rate fields for region II can be obtained by Eq. (3). Since real metals exhibit work-hardening, some modifications are necessary to adapt the theoretical results based on the assumption of perfectly plastic characteristic to the actual process. In this section, we present an extension allowing the consideration of this effect. With the strain rate field and the velocity field, the effective strain can be given as is described in the next section.

2.2 Effective strain

As shown in Fig. 1, each particle of the material undergoes different strains in all three regions. The material undergoes a shear strain at the inlet shear boundary, then it undergoes a strain due to deformation in region II, and respectively it undergoes a shear strain at outlet shear boundary. According to the position of the particle, the total effective strain is obtained for the material and it is substituted in work-hardening model.

In order to obtain total strain, it must be found the strain in each region. The equivalent strain distribution in the rod is determined by integrating the incremental strain along a streamline, shown in Fig. 1.

The engineering shear strain, $\gamma_{s_1}(\beta)$ at the inlet shear boundary is

$$\gamma_{s_1}(\beta) = \left. \frac{\Delta V_\beta}{V_r} \right|_{r=r_o} = \frac{v_o \sin \beta + \frac{v_o r_i}{\partial r} \Big|_{r=r_i} \sin \beta}{v_o \cos \beta} = \left(1 + \frac{r_o}{\tan \alpha} \frac{\partial \psi}{\partial r} \Big|_{r=r_o}\right) \tan \beta \quad (4)$$

where β is the angular position of a particle on the shear boundary S_1 as shown in Fig. 1 and v_o is velocity of initial rod. Assuming proportional distances from die axis of symmetry, the relationship between the angular position β on the shear boundary S_1 and the angular position θ of the particle on a streamline can be generally expressed in the following form, Gordon et al. [8],

$$\frac{\sin \beta}{\sin \alpha} = \frac{\sin \theta}{\sin \psi} \quad (5)$$

The engineering shear strain $\gamma_{s_1}(\beta)$ is transformed into effective strain as:

$$\bar{\varepsilon}_{s_1}(\beta) = \frac{1}{\sqrt{3}} \gamma_{s_1}(\beta) \quad (6)$$

The strain imposed in the deformation region is

$$\bar{\varepsilon}_d(\theta) = \int_{r_f}^{r_o} d\bar{\varepsilon} = \int_{r_f}^{r_o} \frac{d\bar{\varepsilon}}{dt} \frac{dt}{dl} dl \quad (7)$$

where dl is the differential length along the streamline

$$dl = \sqrt{1 + \left(r \frac{d\theta}{dr}\right)^2} dr, \quad \frac{dt}{dl} = \frac{1}{\sqrt{V_r^2 + V_\theta^2}} \quad (8)$$

After substituting

$$\bar{\varepsilon}_d(\theta) = \int_{r_f}^{r_o} \frac{\dot{\bar{\varepsilon}}}{\sqrt{V_r^2 + V_\theta^2}} \sqrt{1 + \left(r \frac{d\theta}{dr}\right)^2} dr \quad (9)$$

where $\dot{\bar{\varepsilon}}$ is the effective strain rate and

$$\dot{\bar{\varepsilon}} = \sqrt{\frac{2}{3} \dot{\varepsilon}_{ij} \dot{\varepsilon}_{ij}} = \frac{1}{\sqrt{3}} \sqrt{3\dot{\varepsilon}_{rr} + 4\dot{\varepsilon}_{r\theta}} \quad (10)$$

By placing Eq. (10) into Eq. (9), we have

$$\bar{\varepsilon}_d(\theta) = \frac{1}{\sqrt{3}} \int_{r_f}^r \frac{\sqrt{3\dot{\varepsilon}_{rr} + 4\dot{\varepsilon}_{\theta\theta}}}{\sqrt{V_r^2 + V_\theta^2}} \sqrt{1 + \left(r \frac{d\theta}{dr}\right)^2} dr \quad (11)$$

The shear strain at the outlet shear boundary S_2 is

$$\gamma_{s_2}(\beta) = \left. \frac{\Delta V_\beta}{V_r} \right|_{r=r_f} = \frac{v_f \sin \beta + \frac{v_f r_f \left. \frac{\partial \psi}{\partial r} \right|_{r=r_f} \sin^2 \beta}{\tan \alpha}}{v_f \cos \beta} = \left(1 + \frac{r_f \left. \frac{\partial \psi}{\partial r} \right|_{r=r_f}}{\tan \alpha} \right) \tan \beta \quad (12)$$

where β is the angular position of the particle on the boundary S_2 . This strain is transformed into the effective strain as:

$$\bar{\varepsilon}_{s_2}(\beta) = \frac{1}{\sqrt{3}} \gamma_{s_2}(\beta) \quad (13)$$

According to the position, the total strain is obtained for the material. The effective strain of the particle on the shear surface S_1 can be given by

$$\bar{\varepsilon}(\theta) = \bar{\varepsilon}_{s_1}(\theta) \quad (14)$$

In deformation domain II the material is in an intermediate state of deformation, the effective strain of the material in the deformation domain, which goes along a streamline, is

$$\bar{\varepsilon}(\theta) = \bar{\varepsilon}_{s_1}(\theta) + \bar{\varepsilon}_d(\theta) \quad (15)$$

The effective strain of the points on the boundary S_2 , the material is completely deformed and we have

$$\bar{\varepsilon}(\theta) = \bar{\varepsilon}_{s_1}(\theta) + \bar{\varepsilon}_d(\theta) + \bar{\varepsilon}_{s_2}(\theta) \quad (16)$$

2.3 Power terms

The internal consumption power, written as:

$$\dot{W}_i = \frac{2}{\sqrt{3}} \int_v \bar{\sigma} \sqrt{\frac{1}{2} \dot{\varepsilon}_{ij} \dot{\varepsilon}_{ij}} dv \quad (17)$$

where $\bar{\sigma}$ is the effective flow stress which it is equal to σ_0 for a perfectly plastic material.

Internal power of regions I and III, are zero and the general equation to calculate the internal power of deformation in region II is calculated as:

$$\dot{W}_i = \frac{2\pi}{\sqrt{3}} \int_{r_f}^{r_0} \int_0^\psi \bar{\sigma} \sqrt{3\dot{\varepsilon}_r^2 + 4\dot{\varepsilon}_\theta^2} (r \sin \theta) r d\theta dr \quad (18)$$

According to the position of each particle, the total strain is obtained for the material and it is substituted in stress-strain relationship in order to modify upper bound method with considering work-hardening. The dissipated shear power on the shear boundary and its relation is

$$\dot{W}_s = \frac{1}{\sqrt{3}} \int_s \bar{\sigma} |\Delta V| dS \quad (19)$$

where ΔV is amount of velocity discontinuity on the shear boundary. Thus, the dissipated shear power on the boundary S_1 is

$$\dot{W}_{S_1} = \frac{2\pi}{\sqrt{3}} r_o^2 \int_0^\alpha \bar{\sigma} |\Delta V_1| \sin \theta d\theta \quad (20)$$

where ΔV_1 is amount of velocity discontinuity on the shear boundary S_1 . For velocity discontinuity surface S_2 , there is. In addition, the dissipated shear power on the boundary S_2 is

$$\dot{W}_{S_2} = \frac{2\pi}{\sqrt{3}} r_f^2 \int_0^\alpha \bar{\sigma} |\Delta V_2| \sin \theta d\theta \quad (21)$$

where ΔV_2 is amount of velocity discontinuity on the shear boundary S_2 . The dissipated friction power at the contact surface of the rod and the die, can be given by

$$\dot{W}_f = \frac{m}{\sqrt{3}} \int_S \bar{\sigma} |\Delta V| dS \quad (22)$$

where m is the constant friction factor between the rod material and the die. After simplification, the dissipated friction power on the frictional surface S_3 , is

$$\dot{W}_f = \frac{2\pi}{\sqrt{3}} m \int_{r_f}^{r_i} \bar{\sigma} |\Delta V_3| r \sin \psi d\psi \quad (23)$$

2.4 The required drawing force

Based on the model, the total required external power for a rod drawing process can be obtained by summing the internal power and the power dissipated on all frictional and shear surfaces, then

$$J^* = \dot{W}_i + \dot{W}_{S_1} + \dot{W}_{S_2} + \dot{W}_f \quad (24)$$

Therefore, the total upper bound solution for drawing force is given by

$$F = \frac{\dot{W}_i + \dot{W}_{S_1} + \dot{W}_{S_2} + \dot{W}_f}{v_f} \quad (25)$$

All the integrals in the above equations do not have analytical solution and have been solved by Simpson's method using MATLAB software. For a given process conditions, the program first calculates the velocity components, the strain rate components, effective strains and then evaluates the upper bound on drawing force, Eq. (25), by numerical integration using the five-point Gauss–Legendre quadrature algorithm. Then, the value of drawing force is minimized with respect to the length of the die profile function.

3 DIE-PROFILE FUNCTION

The shape of the die profile, determines the change of the rod radius in the deformation zone. In the above-developed theory, any possible die shape can be employed, if the die profile is expressed as equation $\psi(r)$. Several different streamlined die shapes are employed in the present investigation as they give less power consumption and good surface finish than conventional conical dies (Gunasekera, Gegel, Malas, Doraivelu, and Barker [12]. The first application of streamlined dies occurred in work by Richmond and Devenpeck [22] to drawing and extrusion of strips. These dies have zero slopes at the die entrance, $r_o \frac{\partial \psi}{\partial r} = -\tan \alpha$, and exit, $r_f \frac{\partial \psi}{\partial r} = -\frac{R_o}{R_f} \tan \alpha$. The

application of the zero slopes at the die entrance and exit, forces the shear power losses over shear surfaces, S_1 and S_2 , to be zero. Geometry of the streamlined dies can be considered as many smooth curves. Four polynomial die profiles are assumed for the die profile. The mathematical representations of these die shapes in cylindrical coordinate system (R, x) are listed in Table 1. Cylindrical coordinate system is used to allow ease of visualization, with R being the radial distance from the axis of symmetry and x the axial distance along the axis of symmetry.

Table 1
The die profile functions in cylindrical coordinate system.

Die shape	Die profile function in cylindrical coordinate system (R, x)
Second order polynomial (Zhang, Chen, Zhou and Zhao [26])	$R(x) = R_0 - 2[(R_0 - R_f)/L^2]x^2$; $R(x) = R_f + 2[(R_0 - R_f)/L^2](x - L)^2$
Third-order polynomial (Chen and Huang [7])	$R(x) = R_0 + (R_0 - R_f)[2(x/L)^3 - 3(x/L)^2]$
Fourth-order polynomial (Yang and Han [24])	$R(x) = R_0 + [C_f L^2 - 3(R_0 - R_f)/L^2]x^2$ $+ [2(R_0 - R_f)/L^3 - 2C_f L]x^3 + C_f x^4$
Fifth-order polynomial (Richmond and Devenpeck [22])	$R(x) = R_0 - (R_0 - R_f)[6(x/L)^5 - 15(x/L)^4 + 10(x/L)^3]$

The equation describes the die shape in spherical coordinate system can be expressed by placing the following equation into the function of the die profile in cylindrical coordinate system as:

$$x = \frac{R_o}{\tan \alpha} - r \cos \psi, \quad R = r \sin \psi \tag{26}$$

4 FINITE ELEMENT ANALYSIS

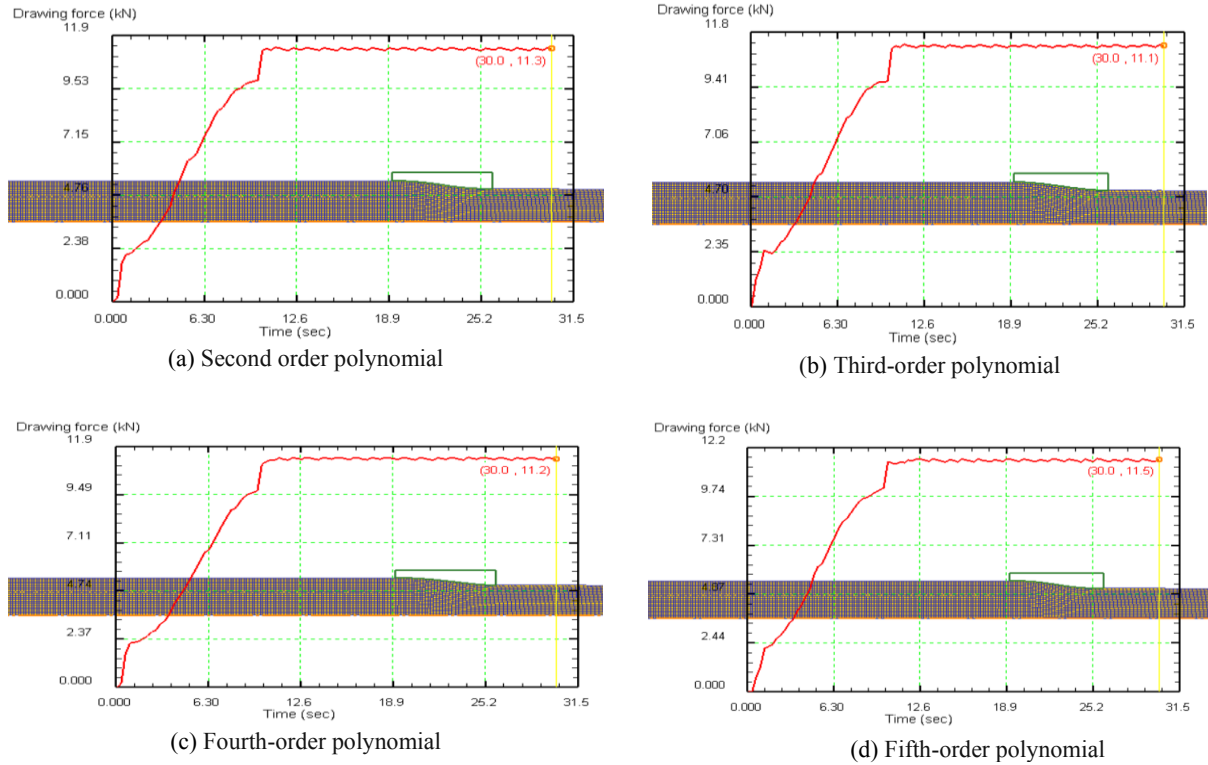
The obvious way to test the validity of the analytical solution developed in the previous sections would be to compare its results with experimental results covering a suitable range of the parameters of interest. Unfortunately, to the best of our knowledge, experimental values of the drawing force are unavailable in literature for rod drawing processes through cured dies. Therefore, one is forced to resort to numerical simulations.

Drawing process is simulated via FEA using DEFORM-2D, a commercial finite element code. Considering the symmetry in geometry, two-dimensional axisymmetric models are used for FEM analyses.

Consider that a rod of initial diameter 10 mm is reduced to final diameter 8 mm, i.e. $\Phi 10 \rightarrow \Phi 8$ drawing process, by using the four different dies as given in Table 1. For all dies, the die length L is assumed to be 10 mm. The element type of the mesh is CAX4R and consists of a 4-node bilinear. These characteristics are appropriate for this element to be used in this type of analysis, where large deformations and nonlinearity contact are assumed. The rod was meshed into 5000 elements. The die is represented by rigid surface elements. The interface between the rod and the die surfaces is represented by interface elements. A constant friction factor 0.05 was used to quantify the friction between the drawing die and rod in the FEM model. The rod velocity was set to 1.0. Default remeshing values were also used. The material has work-hardening behavior and the stress-strain relation is defined by Luis, Leon, and Luri [15]

$$\bar{\sigma}_{cu} = 442(\bar{\epsilon})^{0.117} \text{ MPa} \tag{27}$$

The drawing process has been simulated for different die shapes given in Table 1, by the finite element method. Fig. 2 plots the deformed meshes and the variation of the drawing force during the drawing process for die shapes listed in Table 1, for the case of $\Phi 10 \rightarrow \Phi 8$ drawing process. It is seen that for all die shapes, the drawing force initially increases monotonously until the die is completely filled by the drawn rod. Thereafter, the drawing force remains relatively stable.

**Fig.2**

Deformed meshes and variation of the drawing force during drawing for the a) Second order polynomial, b) Third-order polynomial, c) Fourth-order polynomial, d) Fifth-order polynomial.

5 RESULTS AND DISCUSSION

The effectiveness of the proposed results is demonstrated by comparison with the finite element simulation data. In Table 2, the required drawing force for the case of $\Phi 10 \rightarrow \Phi 8$ drawing process, friction factor 0.05 and die length 10 mm, obtained by upper bound and FEM are compared. The results show a good agreement between the upper bound data and the FE results. Table 2, also shows that the theoretically predicted drawing forces are higher than FE results, shown in Fig. 3, due to the nature of the upper bound theory. It is seen that third-order polynomial die shape has the lowest drawing force, while the largest drawing force has been observed for the fifth-order polynomial die shape. For the third-order polynomial die profile, variation of the drawing force is studied with respect to the friction factor and the work-hardening properties of the drawn material.

Table 2

Comparison between the calculated and FE results of drawing forces.

Die shape	Forward tension	
	Calculated, (kN)	FEM, (kN)
Second order polynomial	11.63	11.3
Third-order polynomial	11.5	11.1
Fourth-order polynomial	11.61	11.2
Fifth-order polynomial	11.8	11.5

The graphs of the drawing force for the third-order polynomial die profile, with only the length as the variable to be optimized, at the case of $\Phi 10 \rightarrow \Phi 8$ drawing process are shown in Fig. 4. Here the variation of the drawing force with die length for two values of the friction factors is given. As shown in this figure, the drawing force decreases with increase in die length up to a certain optimal length and then it increases with increase in die length. As it is expected, for a given value of friction factor, the drawing force is minimized in an optimum die length. For the case of $\Phi 10 \rightarrow \Phi 8$ drawing process and friction factor 0.05, the optimal die length is 8.2 mm and the corresponding die

length for friction factor 0.1 is 6 mm. It is observed that when the friction factor is increased, the optimal die length decreases. This happens to offset the tendency for increase in the frictional power with the die length. This figure also shows that an increase in the friction factor tends to increase the drawing force.

Optimum die shapes for the case of $\Phi 10 \rightarrow \Phi 8$ drawing process for $m=0.05$ and $m=0.1$ are shown in Fig. 4. In this figure, vertical axis shows the radial distance from the axis of symmetry and horizontal axis is the axial distance along the die axis. The differences among the die shapes can be easily noticed.

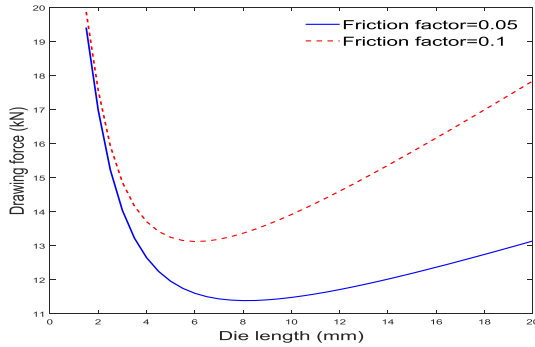


Fig.3
Variations of the drawing force with die length for $m=0.05$, $m=0.1$ for the case of $\Phi 10 \rightarrow \Phi 8$ drawing process.

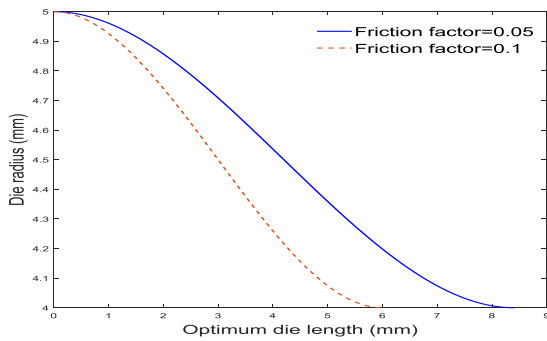


Fig.4
Optimum shapes of the dies for the case of $\Phi 10 \rightarrow \Phi 8$ drawing process for $m=0.05$ and $m=0.1$.

Fig. 5 shows the variation of the drawing force with the die length, for the third-order polynomial die profile, for both perfect plastic and work hardening models for the material at the case of $\Phi 10 \rightarrow \Phi 8$ drawing process and friction factor 0.05. This figure illustrates that the amount of drawing force in the work-hardening model is greater than the perfect plastic model of rod material. It is observed that the optimum die length increases as work hardening of material considers in the solution. These trends are similar to those observed for other optimal curved dies or other materials.

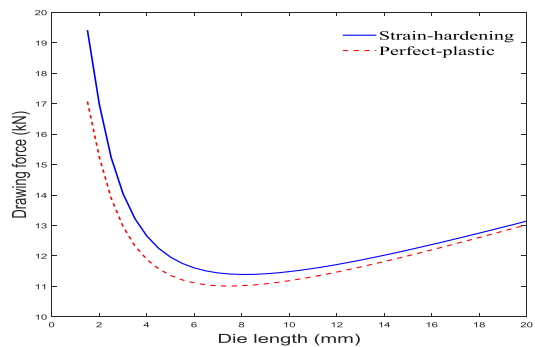


Fig.5
Comparison between variation of drawing force with the die length at the case of $\Phi 10 \rightarrow \Phi 8$ drawing process for friction factor 0.05 assuming perfect and hardening materials.

Fig. 6 shows the effect of work-hardening exponent on the drawing force. It has been demonstrated that material work-hardening exponent has remarkable effect on the required drawing force such that by increasing the work-hardening exponent the drawing force decreases. The reason for this phenomenon is that increasing the work-hardening of a material is equivalent to increasing the sensitivity of its flow stress with respect to the imposed strain. Hence, in such conditions, the rod material would be more susceptible to increase in its flow stress by

developing a small strain. Thus, redundancy becomes the dominant factor in comparison to frictional effect in increasing drawing force, causing the optimum cone angle of each slab to be reduced to minimize the redundancy effect.

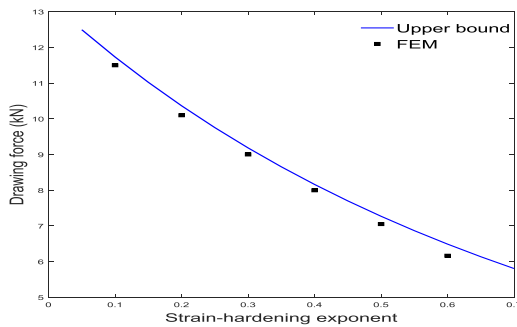


Fig.6

Variation of the drawing force with the work-hardening exponent for $\Phi 10 \rightarrow \Phi 8$ die length 10 mm and friction factor 0.05.

Variation of the optimum die length with work-hardening exponent is represented in Fig. 7 at the case of $\Phi 10 \rightarrow \Phi 8$ drawing process and friction factor 0.05. This figure illustrates that the optimum die length increases by increasing of the work-hardening exponent.

An upper limit to the reduction of area achievable is imposed in a cold drawing process by tensile failure of the drawn product, that is, rupture occurs when the stress in the drawn rod equals or exceeds the maximum tensile stress of the drawn rod. In practice, when a rod is drawn with a reduction in area close to the limiting reduction, the drawn stress is very nearly equal to the maximum tensile stress, so the accuracy of this precept is vitally important. The maximum possible reduction can be obtained as a function of the die length, for several values of the friction factor, equating the drawing stress obtained by the proposed analytical solution of Eq. (8) to the flow stress of the material at the exit of the die, i.e. point P in Fig. 1.

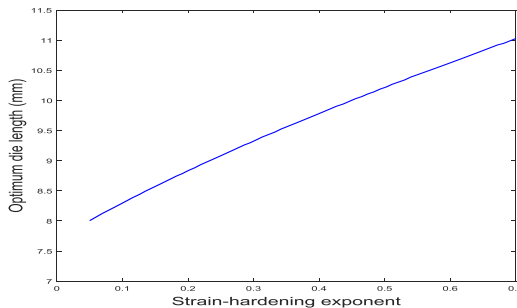


Fig.7

Variation of the optimum die length with the strain-hardening exponent for the case of $\Phi 10 \rightarrow \Phi 8$ and friction factor 0.05.

The maximum values of the reduction in area are plotted in Fig. 8. In this figure, reduction in area for the third-order polynomial die profile obtained from the upper bound solution is compared with each other. Fig. 8 shows the maximum possible reduction for different work-hardening exponents. Points under these curves (corresponding to the drawing stress smaller than the flow stress of the point P) represent possible reductions while those in the neighborhood of the maxima (but still under the curves) correspond to the maximum possible reduction. This figure also shows that maximum value of the reduction decreases when friction factor increases.

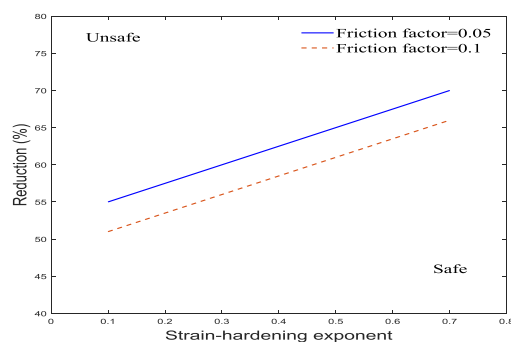


Fig.8

Variation of the maximum reduction value with the work-hardening exponent for the third-order polynomial die profile for friction factors 0.05 and 0.1.

6 CONCLUSIONS

In this paper, an analytical solution is proposed for prediction of drawing force in rod drawing process through curved dies based on upper bound analysis. The developed solution is a function of the material work-hardening exponent value. Through the analysis, following conclusions are obtained:

1. The results afforded by the proposed analytical solution agree with the data from finite element simulations results.
2. The third-order polynomial die profile is superior in comparison to other polynomial die profiles.
3. The amount of drawing force increases when the work-hardening behavior of rod material considers in the solution with respect to the perfectly plastic material.
4. By increasing the work-hardening exponent, the amount of drawing force decreases.
5. The proposed model can be used to design, analyze, and optimize various rod-drawing processes of real materials.

REFERENCES

- [1] Avitzur B., 1963, Analysis of wire drawing and extrusion through conical dies of small cone angle, *ASME Journal of Engineering for Industry* **85**: 89-96.
- [2] Avitzur B., 1964, Analysis of wire drawing and extrusion through conical dies of large cone angle, *ASME Journal of Engineering for Industry* **86**: 305-316.
- [3] Chen C.T., Ling F.F., 1968, Upper bound solutions to axisymmetric extrusion problems, *International Journal of Mechanical Sciences* **10**: 863-879.
- [4] Chen C.C., Oh S.I., Kobayashi S., 1977, Ductile fracture in axisymmetric extrusion and drawing-Part I: Deformation mechanics of extrusion and drawing metal, *ASME Journal of Engineering for Industry* **101**: 369-377.
- [5] Chevalier L., 1992, Prediction of defects in metal forming: application to wire drawing, *Journal of Materials Processing Technology* **32**: 145-153.
- [6] Devenpeck M.L., Richmond O., 1965, Strip drawing experiments with a sigmoidal die profile, *ASME Journal of Engineering for Industry* **87**: 425-428.
- [7] Chen D.C., Huang J.Y., 2007, Design of brass alloy drawing process using Taguchi method, *Materials Science and Engineering* **464**: 135-140.
- [8] Gordon W. A., Van Tyne C. J., Moon Y. H., 2007a, Axisymmetric extrusion through adaptable dies-Part 1: Flexible velocity fields and power terms, *International Journal of Mechanical Sciences* **49**: 86-95.
- [9] Gordon W. A., Van Tyne C. J., Moon Y. H., 2007b, Axisymmetric extrusion through adaptable dies- Part 2: Comparison of velocity fields, *International Journal of Mechanical Sciences* **49**: 96-103.
- [10] Gordon W.A., Van Tyne C. J., Moon Y. H., 2007c, Axisymmetric extrusion through adaptable dies-Part 3: Minimum pressure streamlined die shapes, *International Journal of Mechanical Sciences* **49**: 104-115.
- [11] Gonzalez R.H.A., Calvet J.V., Bubnovich V.I., 2008, A new analytical solution for prediction of forward tension in the drawing process, *Journal of Materials Processing Technology* **198**: 93-98.
- [12] Gunasekera J.S., Gegel H.L., Malas J.C., Doraivelu S.M., Barker D., 1984, CAD/CAM of streamlined extrusion dies, *Journal of Applied Metalworking* **4**: 43-49.
- [13] Liu T.S., Chung N.L., 1990, Extrusion analysis and workability prediction using finite element method, *Computers and Structures* **36**: 369-377.
- [14] Lu Y.H., Lo S.W., 1999, An advanced model of designing controlled strain rate dies for axisymmetric extrusion, *Journal of Materials and Engineering Performance* **8**: 51-60.
- [15] Luis C.J., Leon J., Luri R., 2005, Comparison between finite element method and analytical methods for studying wire drawing processes, *Journal of Materials Processing Technology* **164-165**: 1218-1225.
- [16] Nagpal V., 1974, General kinematically admissible velocity fields for some axisymmetric metal forming problems, *ASME Journal of Engineering for Industry* **96**: 1197-1201.
- [17] Ponalagusamy R., Narayanasamy R., Srinivasan P., 2005, Design and development of streamlined extrusion dies: A Bezier curve approach, *Journal of Materials Processing Technology* **161**: 375-380.
- [18] Panteghini A., Genna F., 2010, An engineering analytical approach to the design of cold wire drawing processes for strain-hardening materials, *International Journal of Materials Forming* **3**: 279-289
- [19] Panteghini A., 2014, An analytical solution for the estimation of the drawing force in three dimensional plate drawing processes, *International Journal of Mechanical Sciences* **84**: 147-157.
- [20] Rubio Alvir E.M., Sebastian P.M.A., Sanz L.A., 2003, Mechanical solutions for drawing processes under plane strain conditions by the upper bound method, *Journal of Materials Processing Technology* **143-144**: 539-545.

- [21] Rubio Alvir E.M., Mariin M., Domingo R., Sebastian P.M.A., 2009, Analysis of plate drawing processes by the upper bound method using theoretical work-hardening materials, *International Journal of Advanced Manufacturing Technology* **40**: 261-269.
- [22] Richmond O., Devenpeck M. L., 1962, A die profile for maximum efficiency in strip drawing, *Proceedings of the Fourth US National Congress of Applied Mechanics ASME1962*, New York.
- [23] Yang D.Y., Han C.H., Lee B.C., 1985, The use of generalized deformation boundaries for the analysis of axisymmetric extrusion through curved dies, *International Journal of Mechanical Sciences* **27**: 653-663.
- [24] Yang D.Y., Han C.H., 1987, A new formulation of generalized velocity field for axisymmetric forward extrusion through arbitrarily curved dies, *ASME Journal of Engineering for Industry* **109**: 161-168.
- [25] Zhao D.W., Zhao H.J., Wang G.D., 1995, Curvilinear integral of the velocity field of drawing and extrusion through elliptic die profile, *Transaction of Nonferrous Metals Society of China* **5**: 79-83.
- [26] Zhang S.H., Chen X.D., Zhou J., Zhao D.W., 2016, Upper bound analysis of wire drawing through a twin parabolic die, *Meccanica* **51**: 2099-2110.